Suppression of Beam-Ion Instability in Electron Rings with Multi-Bunch Train Beam Fillings

L. Wang, Y. Cai and T. O. Raubenheimer, SLAC

H. Fukuma, KEK

The ion-caused beam instability in the future light sources and electron damping rings can be serious due to the high beam current and ultra-small emittance of picometer level. One simple and effective mitigation of the instability is a multi-bunch train beam filling pattern which can significantly reduce the ion density near the beam, and therefore reduce the instability growth rate up to two orders of magnitude. The suppression is more effective for high intensity beams with low emittance. The distribution and the field of trapped ions are benchmarked to validate the model used in the paper. The wake field of ion-cloud and the beam-ion instability is investigated both analytically and numerically. We derived a simple formula for the build-up of ion-cloud and instability growth rate with the multi-bunch-train filling pattern. The ion instabilities in ILC damping ring, SuperKEKB and SPEAR3 are used to compare with our analyses. The analyses in this paper agree well with simulations.

PACS numbers: 29.27.Bd, 29.20.db

I. INTRODUCTION

In accelerators with negatively charged beams, an electron accelerator for instance, ions generated from the residual gas molecules can be trapped by the beam. The trapped ions interact resonantly with the beam and cause a beam-ion coherent instability, tune shift, and emittance blow-up[1~3]. This beam-ion instability can occur in both ring and linac [4]. Besides the electron accelerator, the beam ion instability can also occur in other negatively charged beams, including the antiproton beam [5]. This paper studies the beam-ion instability in an electron ring only. A similar method can be used to study the instability in a linac.

"Conventional" ion-effects occur when ions are trapped by a circulating electron beam for multiple revolutions. To avoid conventional ion trapping, a long gap is introduced in the electron beam. However, such a gap does not preclude ions from accumulating during one passage of the single bunch train beam, and those ions can still cause a Fast Ion Instability (FII) [6-9], especially in long storage rings where a single bunch train can be long enough to trap enough ions and cause FII.

Work supported in part by US Department of Energy contract DE-AC02-76SF00515.

SLAC National Accelerator Laboratory, Menlo Park, CA 94025

Beam shaking is an effective way to make the ion unstable [10]. However, the required shaking amplitude should be larger than the beam size. Such a disturbed beam cannot be used. The alternate way to avoid trapped ions is to introduce clearing electrodes. A minimum condition for the capture of the passing ion is that the transverse field potential provided by the electrode equals the maximum beam's space charge potential, which is typically more than 1 *kVolt*. Because a clearing electrode can only clear ions nearby, the required number of clearing electrode is large for a long storage ring. Furthermore, the clearing electrode complicates the mechanical design of the vacuum chamber and also contributes to the machine impedance [11]. For a small ring, this is an effective mitigation; for instance, the Beam Position Monitor (BPM) can be used to clear ions.

This paper studies the suppression of beam-ion instability by simply using multi-bunch train filling patterns. As shown late that the instability growth rate is proportional to the ion density at the beam. Therefore, it is important to reduce the ion density in the vicinity of the beam to a tolerable level. Single bunch train filling pattern is used in B-factory and most existing light sources. Numerical studies show that a multi-bunch train with short gaps is very effective at reducing the ion density near the beam [12]. These short gaps in the filling pattern lead to an absence of focusing forces for the ions every time the gaps travel around the ring. The beam force over-focuses ions and permits them to oscillate to large amplitudes out of the beam center. However, no analysis has been done understand the mechanism. It is practically important to have the analysis done to guide the operation on how to choose beam filling pattern.

The beam ion instability in ILC has been simulated in previous papers [13, 14]. This study focuses on the physical understanding, instead of simulation. The example of the numerical and experimental results for ILC damping ring, SuperKEKB and SPEAR3 are used to compare with our analysis. Although our approaches are similar with the one used in the study of electron cloud and instability driven by traditional impedance, it is far from being a mere repetition of already known results. In fact our analysis will rove superior when it comes to physical understanding and accuracy of approximation: it has important application in estimation of practical quantities.

This paper systematically studies beam instability with multi-bunch train beam filling. The simple physical model considered in this paper gives simple analytical relations. Such a model allows one to obtain a deeper insight into the physics of beam ion instability with a general beam filling pattern. This

paper is organized as follows. The transverse distribution and the fields of trapped ion are investigated in section II. In section III, we describe the interaction force between the electron beam and ions using conventional wake and give the instability growth rate for uniform and single bunch train filled beam, respectively. The mechanism of the mitigation of beam instability by using multi-bunch train beam filling pattern is investigated in great detail in section IV. Simple formulae for the build-up of ion cloud and instability growth rate are given. The ion-cloud induced tune shift and the suppression of beam instability using bunch-by-bunch feedback are briefly discussed in section V. Finally, in section VI we come to conclusions.

II. TRANSVERSE DISTRIBUTION AND FIELD OF AN ION CLOUD

It is important to investigate the distribution and the field of trapped ions. A few of works about the ion distribution have been done [15] comparing a larger number of publications in the instabilities [6-9]. For completeness, we briefly analyze the distribution of trapped ions in steady status in Appendix. One can refer to Tavares early work for more detail [15].

The one dimensional transverse distribution of ions trapped by the electron bunches at the equilibrium state is

$$\rho(x) = \frac{1}{\pi\sqrt{2\pi}\sigma_{e,x}} e^{-\frac{x^2}{4\sigma_{e,x}^2}} K_0\left(\frac{x^2}{4\sigma_{e,x}^2}\right), \tag{1}$$

where K_0 is the modified Bessel Function of the Second Kind, σ_e is the transverse root mean square (*rms*) beam size of the electron bunch from which the ions are born. The asymptotic forms of ion distribution near the beam center is

$$\rho(x) \approx -\frac{1}{\pi\sqrt{2\pi}\sigma_{e,x}} e^{-\frac{x^2}{4\sigma_{e,x}^2}} \left(\log(\frac{x^2}{8\sigma_{e,x}^2}) + \gamma_c\right). \tag{2}$$

The same result in Eq. (1) is first given by Tavares [15]. However the asymptotic form in [15] is incorrect.

Fig.1 compares the ion distributions from analytical and numerical methods. There is an excellent agreement except at the origin where the analytical result diverges. There is a sharp peak near the center because the ions are sharply focused to that point and the size of the ion cloud is smaller than that of the electron bunch. The result given in Eq.(1-2) works in linear regime. Surprisingly, it agrees well with simulation. This probably is because most ions are focused near the beam center where the linear model works. Fig. 2 shows the two-dimensional distribution of ion-cloud by simulation. Note that the transverse position in the figure is in the unit of beam size. The transverse distribution of ion cloud is very flat for most light sources due to a small coupling.

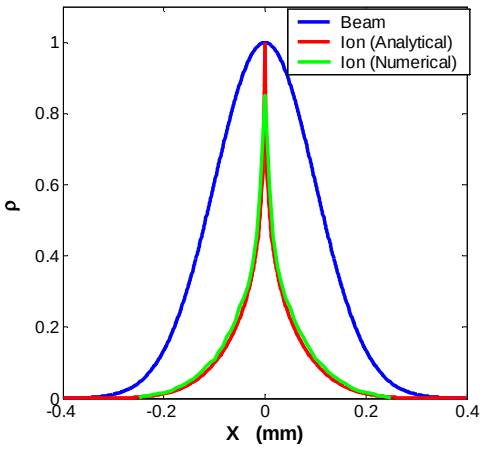

FIG. 1. Comparison of the ion distribution from analytical and numerical approaches. The electron beam profile is also shown in the plot for a better comparison. The *rms* beam size is 0.1 *mm* and 4.5 μm in horizontal and vertical planes, respectively.

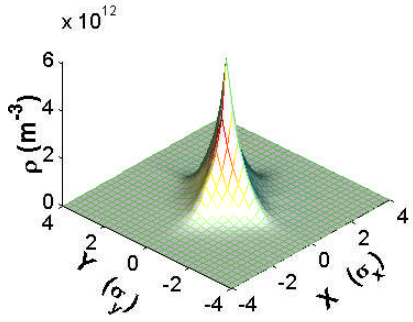

FIG. 2. Two dimensional distribution of an ion cloud from simulation. X and Y are in the unit of *rms* beam size

Since the distribution of the ion cloud is special, there is no available formula to calculate the field of such distributed charged particles. The formula for calculating electric field of a Gaussian beam is well known and an ion cloud with Gaussian distribution has been assumed in the previous analysis of the beam ion instability [6-8]. However, this assumption has never been benchmarked. Fig.3 shows a comparison of the electric field of an ion cloud shown in Fig. 2 with the field of a Gaussian distributed ion cloud with a *rms* size of $\sigma_i = \sigma_e / \sqrt{2}$. The different lines in Fig. 3 are for different horizontal positions. It is clear that the fields of these two distributions are quite similar overall. The field with a distribution shown in Fig. 2 is slightly stronger and has a larger gradient near the center. In short summary, it slightly under estimates the ion effects by the assumption of a Gaussian distribution with $\sigma_i = \sigma_e / \sqrt{2}$. This assumption will be used in the rest of this paper. As shown late the wake and the tune shift due to the trapped ions with this assumption reasonably agree with simulations.

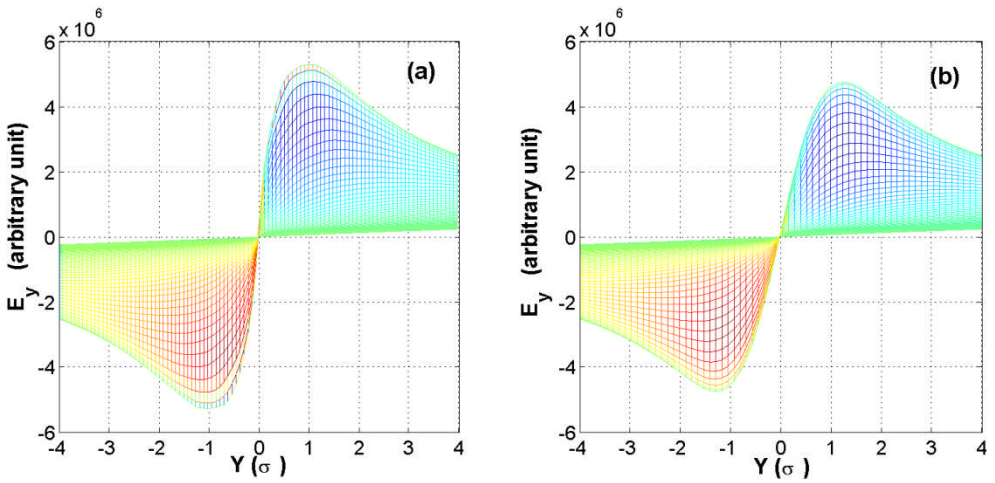

FIG. 3 Vertical electric field of an ion cloud shown in Fig.2 (a) and an Gaussian distributed ion cloud with $\sigma_i = \sigma_e / \sqrt{2}$ (b). The total charge is the same for the two distributions. Different lines in the figures are for different *x*. Y is in the unit of *rms* beam size

III. WAKE FIELD AND GROWTH RATE OF THE COUPLED BUNCH INSTABILITY DRIVEN BY IONS

The two stream instability driven by electron cloud has been studied using wake model [16]. The distribution of the electron cloud was assumed to be Gaussian in transverse plane and a coasting beam model was used for the positron beam. The wake due to electron cloud in a magnetic field free region is short range wake and can cause head-tail instability [17]. However the ion cloud has special distribution and the electron beam is bunched beam. The wake of ion cloud is long range wake due to the heavier mass of ions and therefore it may drive coupled bunch instability. The wake of ion cloud given in [14] used a wrong ion distribution model. The distribution of ions was simply assumed to be the same as the electrons and their result is inaccurate. Therefore the wake of ion cloud is well worth careful study and evaluation. In this section we investigate the wake due to ions in great detail and validate it with numerical simulation.

When the charged electron beam passes through the vacuum chamber, ions are generated due to the beam-gas ionization. For a single bunch train consisting of n_b bunches followed a long gap, the ion line density at the tail of the bunch train is given by

$$\lambda_i = \delta_i \frac{P}{kT} N_e n_b \ . \tag{3}$$

Here P is the vacuum pressure, δ_i is the ionization cross-section, N_e is the number of electrons per bunch, T is temperature and k is Boltzmann constant.

We ignore the self direct space charge effects, such as the effect of the ion fields on the ions and the effect of electron beam field on the electrons. We are interested mainly in the coupled motion of the ions and the electron beam.

The dipole kick of ion-cloud to the electron bunches can be expressed as the direct space charge force [6, 7]. One alternate approach is to express the kick using a wake function model, which allows the beam-ion instability to be studied in the same way as the coupled bunch instability driven by traditional impedance. When the electron bunches pass through the center of the ion-cloud, they are not affected by the ion-cloud due to the symmetry of the ion distribution, and the center of mass of the ion cloud does not move. However, if a bunch with a small transverse displacement passes through the cloud, the cloud is disturbed and its center of mass starts to oscillate. Then, the subsequent bunches are deflected by the perturbed ion-cloud. The wake force of the ion-cloud is calculated as the response to a small displacement of i^{th} bunch Δy_{e0},

$$W_y(z_j - z_i) = \frac{\gamma}{N_e r_e} \frac{\Delta \bar{y}'_{ej}}{\Delta y_{e0}} \quad \text{for} \quad z_i < z_j \ , \tag{4}$$

where r_e is the classical radius of electron and γ is the relativistic factor, and $\Delta y'_{ej}$ is the kick of ion-cloud to the j^{th} electron bunch.

When the offset Δy_{e0} is smaller than the beam size, the ion-cloud receives a linear kick

$$\Delta \upsilon_{yi} = \frac{N_e r_p c}{A} \frac{2}{\sum_y (\sum_x + \sum_y)} \Delta y_{e0} \, , \tag{5}$$

where r_p is the classical radius of proton, A is the mass number of the ion, c is the speed of light, and the cross sectional area is given by

$$\sum_x = \sqrt{\sigma_{e,x}^2 + \sigma_{i,x}^2} \ , \ \sum_y = \sqrt{\sigma_{e,y}^2 + \sigma_{i,y}^2} \ . \tag{6}$$

Here σ_i is the transverse size of the ion-cloud. The kick triggers the oscillation of the ion-cloud at amplitude

$$\hat{y}_i = \frac{\Delta \upsilon_{yi}}{\omega_{i,y}} = \frac{N_e r_p c}{\omega_{i,y} A} \frac{2}{\sum_y (\sum_x + \sum_y)} \Delta y_{e0} \,. \tag{7}$$

Here $\omega_{i,x,y}$ is the oscillation frequency of the ion-cloud under the space charge force of the electron beam

$$\omega_{i,x,y} = c \left(\frac{2\lambda_e r_p}{A k_{x,y} \sigma_{x,y} (\sigma_y + \sigma_x)} \right)^{1/2} \,. \tag{8}$$

Then the following electron bunches receive a kick from the oscillating ion-cloud

$$\Delta y'_e = \frac{\Delta \upsilon_{ye}}{\gamma c} = \frac{N_i r_e}{\gamma} \frac{2}{\sum_y (\sum_x + \sum_y)} y_i \,, \tag{9}$$

where N_i is the number of ions. Substituting Eq.(9) and (7) into eq. (4), the maximum kick received by electron bunches gives the amplitude of the wake

$$\hat{W}_y = \frac{2}{k_y} \frac{\omega_{i,y}}{c} \frac{N_i}{\lambda_e} \frac{1}{\sigma_y (\sigma_y + \sigma_x)} = N_i \left(\frac{r_p}{A \lambda_e} \right)^{1/2} \left[\frac{2}{k_y} \frac{1}{\sigma_y (\sigma_y + \sigma_x)} \right]^{3/2} \,. \tag{10}$$

Where $\lambda_e = N_e / S_b$ is the line density of electron bunch and S_b is bunch spacing. The parameter $k_{x,y} = \sum_{x,y} (\sum_x + \sum_y) / (\sigma_{x,y} (\sigma_y + \sigma_x))$ is derived from the integration over two Gaussian distributions, representing the beam and ion-cloud. As shown in the last section, the transverse distribution of ions is not Gaussian, but the electric field of the ion-cloud closely approximates that of a Gaussian distribution with $\sigma_i^2 \approx \sigma_e^2 / 2$. Therefore, $k_x = k_y \approx 3/2$ with this approximation. For a flat beam, the vertical wake is stronger than the horizontal one. Therefore, there is a stronger instability in the vertical direction. We will discuss the instability in the vertical direction only in the rest of this paper and omit the subscript *y* in some variables for simplicity.

Note that the wake of ions given by [14] differs from our result shown in Eq.(10) by a factor of 4/3. The ion frequency in [14] is also different from ours and others [6-7] by a factor of 2/3. Our model is more accurate and has good agreement with simulation as shown late.

Due to the nonlinear space charge force between electron beam and ion-cloud, the wake of the ion-cloud has a finite quality factor *Q* which characters the frequency spread of the individual ions. Therefore, more precisely, the wake of ion-cloud has the following form

$$W(z) = \hat{W}\, e^{-\frac{\omega_i z}{2Qc}} \sin(\frac{\omega_i z}{c}) . \tag{11}$$

Fig. 4 shows the simulated wake of ion-cloud for various offsets of the test bunch Δy_{e0}. The test bunch initially has a vertical offset Δy_{e0} (for the vertical wake calculation) and the following bunches have zero offset. The ion cloud is disturbed by the test bunch due to the offset and then starts an oscillation. The oscillated ion cloud gives a vertical kicker to the following bunches $\Delta y_e'$. The wake is calculated as $W_y(z) = \gamma \Delta y_e'(z) / (N_e r_e \Delta y_{e0})$. Here *z* is the distance between the test bunch and the bunch which receives the kicker from the ion cloud. The wake is insensitive to Δy_{e0} when Δy_{e0} is smaller than the beam size, which means the electric field of the ion-cloud has good linearity. However, when the bunch's offset is larger than the beam size, the wake becomes smaller and has strong nonlinearity due to the nonlinear field shown in Fig. 3. Therefore, the above wake model works well only in the linear regime, where the fast instability occurs as shown by the simulations in the following section; hence the model of the wake can still give the most important information about the beam-ion instability.

The wake of ion-cloud is a long range wake due to the heavy mass of the ions. For instance, the frequency of wake due to ion-cloud in SPEAR3 ranges from a few of *MHz* to 70*MHz* in the 500*mA* operation mode. The frequency depends on the ion species and also varies along the ring due to the variation of the beam size. The wavelength of the wake can be larger as 30.0 *m* (10MHz) while the bunch spacing is only 0.63*m*.

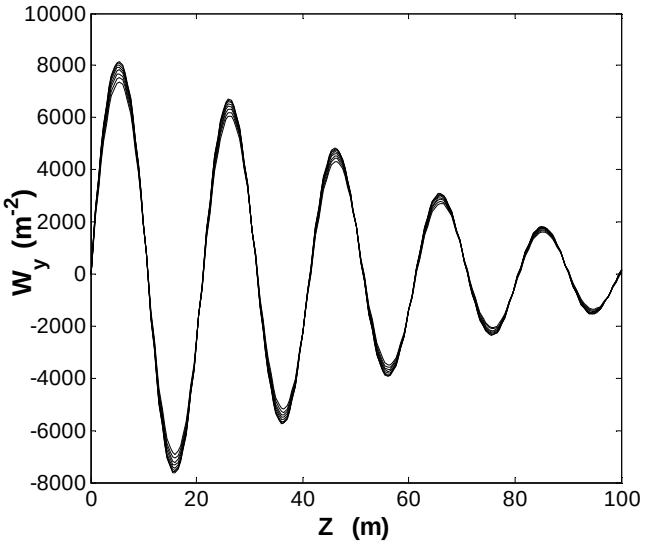

FIG. 4. Simulated wake of ion-cloud for various Δy_{e0} ranging from 0.1 σ to 1 σ with a step of 0.1σ. The beam parameters are σ_x=*1.19mm,* σ_y=*7.56μm,* N_e=5×10^9 , S_b=*0.5m* and *A*=28 (CO^+).

Fig. 5 shows the simulated wake field for different bunch spacing with a constant beam line density λ_e. For instance, the bunch intensity doubles when the bunch spacing is doubled. The number of ions is the same in all cases. It clearly shows that the wake field does not depend on the bunch spacing; instead, it depends on the beam line density. This agrees well with the analytical model.

Fig. 6 compares the wakes by numerical and analytical approaches. A *Q* of 9 is assumed for the analytical method. There is a good agreement in both frequency and amplitude. Note that the analytical approach used an approximation model of the ion's distribution and dimension. The simulated wake can also be fitted using the form of Eq. (11) to get the amplitude, frequency and Q. For example, the fitted parameters of the simulated wake in Fig. 5 are: $\hat{W} = 9827 m^{-2}$, *Q*=9, and $\omega_i = 92 MHz$. The analytical formula gives $\hat{W} = 9671\, m^{-2}$ and $\omega_i = 84.95 MHz$. The frequency and amplitude from analysis approach are 8% and 16% smaller than the simulated ones, respectively. This is fundamentally consistent with the field comparison shown in Fig. 3. Previous analysis result gives a *Q* of 16 [7], which is larger than the numerical one. Fig. 7 shows the dependence of the amplitude and frequency of the wake on the beam line density by simulation. The amplitude, frequency and *Q* are found by fitting the wake with the model in Eq. (11).

Simulation shows that the Q doesn't change with beam line density. As shown in the figure, both amplitude and frequency linearly increases with the square root of the beam line density.

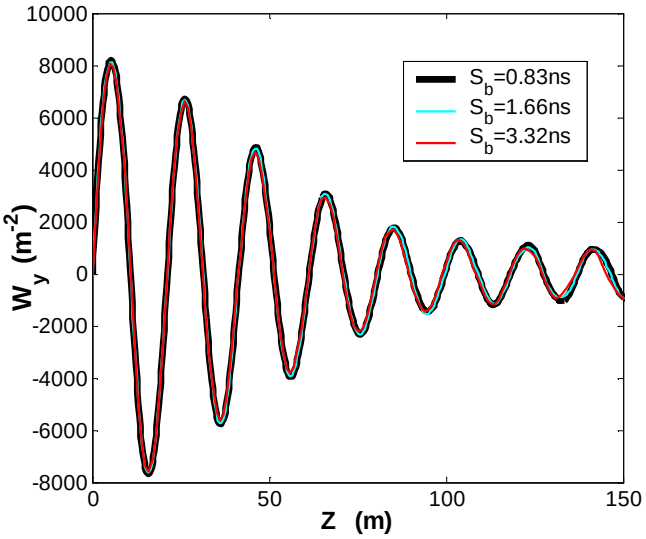

FIG. 5. Wake of ion-cloud for various bunch-spacing with a constant beam line density and number of ions.

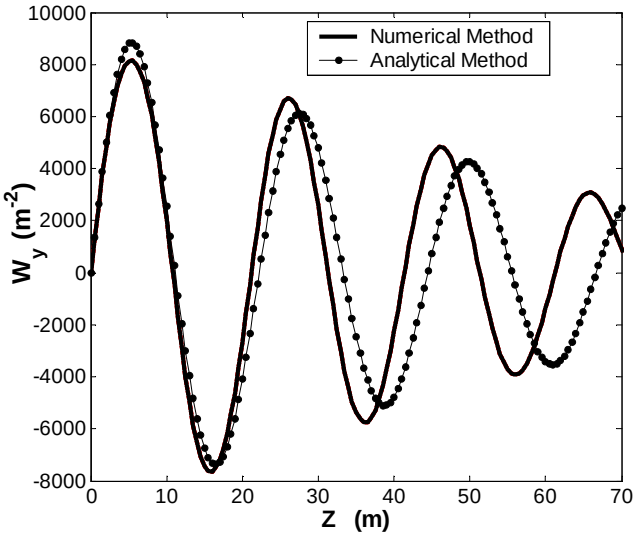

FIG. 6. Comparison of the wake due to ion-cloud given by numerical and analytical methods, $\Delta y_{e0} = 0.13\sigma$ is used in the simulation and Q=9 is used in the analysis.

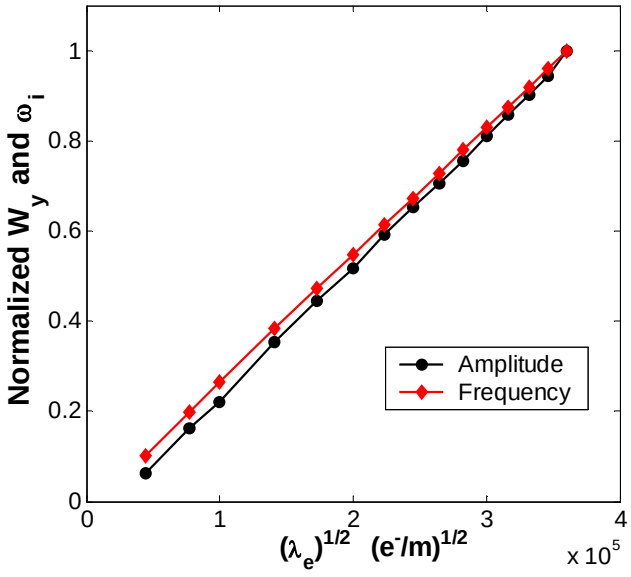

FIG. 7. Dependence of the amplitude and frequency of the wake on the beam line density by simulation. Both the amplitude and frequency is normalized in order to clearly display both of them in one plot. The beam filling pattern is single bunch train.

In summary, the wake field of an ion-cloud has the following characteristics:

- When the wavelength of ion oscillation is much longer than the bunch spacing, the wake (both frequency and amplitude) depends on the average beam line density λ_e, instead of the bunch spacing or the bunch current. In other words, the wake depends on the average force of the electron beam because the ions move slowly.
- Its frequency is the same as the ion's oscillation frequency, which is proportional to the square root of the beam line density as shown in Fig. 7.
- The amplitude of the wake is proportional to the line density of ion-cloud and inversely proportional to the square root of the beam line density. For a single bunch train filling pattern, the ion density is proportional to the beam density. Therefore, the wake is ultimately proportional to the square root of the beam line density: $\hat{W} \propto \lambda_e^{1/2}$ as shown in Fig.7.
- For a flat beam ($\sigma_x >> \sigma_y$), $\hat{W} \propto \sigma_x^{-3/2}\sigma_y^{-3/2}$. Therefore, there is a strong wake for a small beam.

- The model of wake works only in the linear region as expected. When the amplitude of a bunch's oscillation is larger than the beam size, the force received by the electron bunches has strong nonlinearity, which slows down the instability as shown late by simulation. Since the fast instability occurs in the linear regime, the wake model is very useful to estimate the fast growth rate.
- The nonlinearity of the ion-cloud gives a small Q which is normally less than 10.

With an assumption of a constant ion line density and beam size along the ring, the total wake field due to the ion-cloud in the whole ring can be written as

$$W_{y,total}(z) = \hat{W}_t e^{-\frac{\omega_i z}{2Qc}} \sin(\frac{\omega_i z}{c}), \tag{12}$$

with the amplitude of the wake

$$\hat{W}_t = \frac{2\omega_i}{c}\frac{L}{\lambda_e}\rho_{i,eff}, \tag{13}$$

where L is the circumference of the ring and $\rho_{i,eff}$ is the effective ion density, which is defined as

$$\rho_{i,eff} = \frac{\lambda_i}{k_y \sigma_y(\sigma_y + \sigma_x)}. \tag{14}$$

There is a flat beam for most electron rings with $\sigma_x >> \sigma_y$. The factor of $1/k_y$ in the effective ion density represents the dependence of wake on the ion's distribution.

In the above discussion, a constant beam size is used to estimate the total wake of the ring. The total wake of a ring should be found by integration along the ring to include the variation of the beam size. Moreover, the motions of ions in both horizontal and vertical directions are assumed to be stable. If the ion's motion is unstable, the ion density becomes smaller.

The Fourier transformation of the wake gives the impedance in the frequency domain as

$$Z_{ion}(\omega) \approx \frac{\hat{W}_t}{\omega}\frac{Q}{1+iQ\left(\frac{\omega_i}{\omega}-\frac{\omega}{\omega_i}\right)}. \tag{15}$$

When the beam is evenly filled along the ring, the exponential growth rate of the coupled bunch instability for mode $y_j^{\mu} \propto e^{2\pi\mu j/n_b}$ is [18]

$$\frac{1}{\tau^{\mu}} = \frac{N_e n_b r_e c}{2\gamma T_0^2 \omega_\beta}\sum_{p=-\infty}^{\infty}\mathrm{Re}\left[Z_{ion}((pn_b + \nu_y + \mu)\omega_0)\right]. \tag{16}$$

Here ν_y and ω_β are the betatron tune and frequency, T_0 and ω_0 are revolution period and frequency. At the resonance, $\omega = \omega_i$, the real part of the effective impedance can be simplified to

$$\mathrm{Re}\sum_{p=-\infty}^{\infty} Z_{ion}((pn_b + \nu_y + \mu)\omega_0) \approx \frac{\omega_i}{\omega} R = \frac{\hat{W}_t}{\omega_i} Q \quad . \tag{17}$$

This gives a maximum growth rate

$$\frac{1}{\tau} \approx \frac{r_e c \beta_y \rho_{i,eff} Q}{\gamma} = \frac{r_e c \beta_y Q}{\gamma} \frac{\lambda_i}{k_y \sigma_y (\sigma_y + \sigma_x)} \quad . \tag{18}$$

The relationships $\omega_\beta T = L/\beta_y$ and $L\lambda_e = LN_e / S_b = N_e n_b$ are used in the above derivation.

The frequency of the wake depends on the transverse beam size. Accordingly, the variation of the betatron function along the storage ring induces a frequency spread. This frequency spread results in a reduction of the effective Q of the wake. For instance, the exponential growth rate of the fast ion beam instability of single bunch train beam with a frequency variation of $\Delta\omega_i$ due to the change of beam size is [8]

$$\frac{1}{\tau_{e,FII}} \approx \frac{r_e c \beta_y \lambda_i}{3\sqrt{2}\gamma \sigma_y (\sigma_y + \sigma_x)} \frac{1}{\Delta\omega_i / \omega_i}, \tag{19}$$

here λ_i is the ion line density at the end of the bunch train. The frequency variation of $\Delta\omega_i$ has a similar landau damping mechanism as the nonlinear space charge effect in Eq. (18). If we define an effective Q due to this frequency spread as

$$Q_{optics} = \frac{\omega_i}{\sqrt{2}\Delta\omega_i}, \tag{20}$$

For example, an optics with $\Delta\omega_i/\omega_i$=0.2 gives a Q_{optics} of 3.54. Then Eq. (19) can be re-written as

$$\frac{1}{\tau_{e,FII}} \approx \frac{1}{2} \frac{r_e c \beta_y \rho_{i,eff} Q_{optics}}{\gamma}. \tag{21}$$

The two types of instability represented in Eq. (18) and Eq. (21) have the same form except a factor of ½ in the FII case which gives the average density along the bunch-train. Note that the ion density linearly increases along the bunch train for single bunch train case. If we use the average ion density over the bunch train, the two equations will be identical: the growth rate is proportional to the average effective ion density near the beam

$$\frac{1}{\tau} \approx \frac{r_e c \beta_y \bar{\rho}_{i,eff} Q}{\gamma} \quad . \tag{22}$$

Roughly speaking, the frequency spread due to the optics and the nonlinearity of ion-cloud has the equivalent effect in damping the instability. Q in the above equation can include both effects.

There are multi-gas species in the beam's vacuum chamber. The dominant species are Hydrogen, Methane, Water, Carbon Monoxide and Carbon Dioxide in most electron rings. Each type of ion has its own frequency and frequency spread due to the variation of beam size along the ring. Therefore, additional

tune spread may be added when multi-species are considered. This effect is mixed with the trapping condition, train gap effect and optics effect. Simulation of the ILC damping ring shows that the additional damping effect due to multi-gas species is small [19]. Another simulation concludes that the superposition rule applies for multi-species of ions [9]. In this case, one can independently calculate the growth rate due to individual gas species. Note that the growth rate doesn't depend on the ion frequency, but the unstable mode number does. The superposition rule may fail for some rings. Detail parameters need to be checked for each case. For most electron rings, the frequency of Hydrogen is well separated from the frequencies of other types of ions. As a result, Hydrogen doesn't contribute to additional frequency spread. The frequencies of Carbon Monoxide and Carbon Dioxide are close to each other. They may overlap due to the variation of the beam size along the ring and result in an increment of the total frequency variation.

IV. MITIGATION OF THE BEAM INSTABILITY WITH MULTI-BUNCH TRAIN BEAM FILLING

Table 1 compares the main parameters and the driving force of the beam-ion instability in several existing and designed electron rings. The emittance of the future rings is up to two orders of magnitude smaller than the present B-factory. Note that a constant beam size is used for each ring and the trapping condition is not applied. The last column shows the normalized $\rho_{i,eff}/\gamma$ with the assumption of one single bunch train beam filling pattern. The value of $\rho_{i,eff}/\gamma$ in KEKB is assumed to be 1. With the single bunch train beam, the ion density is proportional to the total number of electrons in the ring. Among the listed existing rings, SSRF, KEK ATF, SPEAR3 and SLS have relatively strong instability due to their small beam size. The beam ion instability has been observed in PLS [20], SOLEIL [21], SSRF [22] and SPEAR3. Vertical emittance blow up has been observed in Australian Synchrotron (AS) [23], which could be an indication of the beam ion instability. Beam ion instability hasn't been reported in SLS with normal operation filling pattern. But it is expected according to our first order estimation listed in Table 1. A detail simulation is necessary to evaluate the beam ion instability in SLS. Two options for SUPERKEKB are listed: the high charge option (SUPERKEKB I) and low charge with low emittance option (SUPERKEKB II). The low charge option has stronger instability due to its small emittance. The ultra-small emittance in the PEPX [24] can drive the strongest beam instability. The beam ion instability is not a problem for most

of the existing electron rings. However, it can be a serious problem for the future rings with high beam current and small emittance as shown in Table 1.

In order to mitigate the instability, one direct solution is to reduce the ion density near the beam. A low ion density can be achieved using a clearing electrode, a better vacuum, or beam shaking. Here we study one simple and effective way to reduce ion density by using a multi-bunch-train beam filling pattern. The instability with a gap is studied in [25, 26].

Table 1: Comparison of main parameters and driving force of beam-ion instability in existing rings and future rings (underlined). Single bunch beam filling pattern and constant vacuum pressure are assumed in the comparisons. The average betatron function is used in the estimation of the beam size.

RING	E (GeV)	Cir(m)	n_b	I (mA)	L_{SP}(m)	e_x/σ_x nm·rad/μm	e_y/σ_Y nm·rad/μm	$\rho_{i,eff}/\gamma$
PEPII	8.0	2199	1588	1550	1.26	31/660	1.4/144	1.1
KEKB	8.0	3016	1387	1200	2.1	24/500	0.49/75	1.0
ALS	1.5/1.9	196.8	320	400	0.6	6.3/160	0.06/23	1.2
APS	7.0	1104	24	100	45.9	3.0/276	0.025/11	0.4
PLS	2.0	280	180	360	0.6	12.1/350	0.12/35	0.3
AS	3.0	216	300	200	0.6	10.3/165	0.03/14	0.5
SSRF	3.5	432	450	200	0.6	3.9/110	0.0273/13	1.4
KEK ATF	1.3	138	20	64	0.77	1.2/70	0.0045/5	1.6
SPEAR3	3.0	234	280	500	0.63	10/200	0.014/10	1.6
SLS	2.4	288	390	400	0.6	5.5/111	0.005/5.6	6.4
NSLSII	3.0	792	1040	500	0.6	1.0/122	0.008/11	8.1
SUPERKEKB I	3.5	3016	5120	9400	0.6	24/600	0.24/60	18.7
SUPERKEKBII	7.0	3016	2500	2600	1.18	5.1/280	0.013/14	23.7
ILC	5.0	6000	3000	400	0.5	0.8/120	0.002/6	55.3
PEPX	4.5	2199	3154	1500	0.6	0.08/18	0.0043/5.7	596

Diffusion of ion-cloud during the train gap

We begin with ion's single particle motion under the potential of electron beam. In the linear regime, the Hamiltonian for an ion is

$$H(x, p_x, y, p_y) = \frac{p_x^2}{2m_i} + \frac{p_y^2}{2m_i} + \frac{1}{2} m_i \omega_{i,x}^2 x^2 + \frac{1}{2} m\, \omega_{i,y}^2 y^2 \ . \tag{23}$$

Here m_i is the mass of ion. The ions initially have the same distribution as the electrons. A good approximation is obtained by assuming that the ions are born at zero velocity since the beam's potential is much larger than the ions' thermal energy. Therefore, the displacement and velocity of the ion in the vertical direction follow

$$y(t) = y_0 \sin(\omega_i t + \phi_0) \ , \tag{24}$$

$$\upsilon(t) = y_0 \omega_i \cos(\omega_i t + \phi_0) \ , \tag{25}$$

where y_0 is the ion's oscillation amplitude, which is approximately the position at its birth. ϕ_0 is the ion's initial phase when the ions are born, which has a uniform distribution due to the random process of ionization. Hence, the ion's speed has the following distribution

$$f(\xi) = \frac{2}{\pi} \frac{1}{\sqrt{1-\xi^2}}, \tag{26}$$

where $\xi = \upsilon / \omega_i y_0$. The distribution is shown in Fig.8. It is seen from this plot that the distribution has a sharp peak at the maximum speed. During the bunch train gap, the ions drift with constant velocity (ions' self-space charge effect is negligible). The speed distribution in Eq. (26) indicates that the ion density near the beam decay fast at the beginning and then slows down. Fig. 9 shows the simulated build-up of ions near the beam and its decay during the train gap. The ion density linearly increases along the bunch train. During the train gap it is roughly an exponential decay with a decay time order of the ion's oscillation period. This can be explained by Eq. (25), which shows ions with a short oscillation period drift quickly during the gap. The experiment in SPring-8 also shows a similar exponential decay of the ion density, beam size and betatron tune shift during the train gap [27].

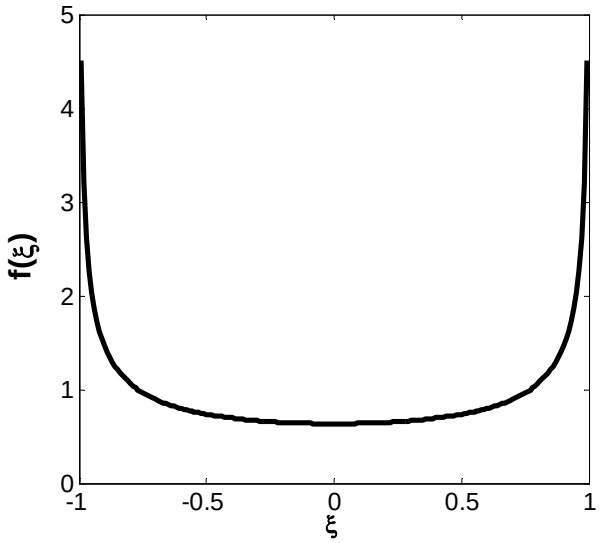

FIG. 8. Distributions of the speed of ion particles.

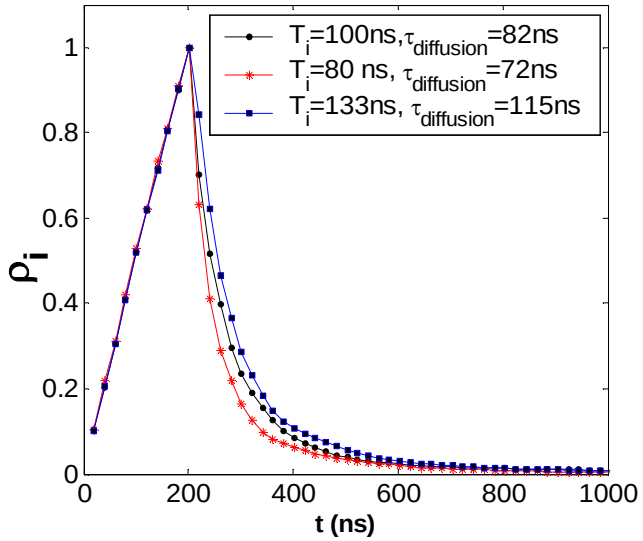

FIG. 9. Build-up of ion-cloud along a short bunch train and its decay during the train gap for various ions' oscillation frequencies. The ion density is normalized so that the peak density at the end of the bunch train is 1. The calculated ion oscillation period T_i and the simulated ion decay time $\tau_{diffusion}$ during the bunch train gap are also shown in the plot.

The linear motion of ions with a bunch-train gap can also be studied using a transportation matrix. The ion receives a linear kicker during the passage of an electron bunch (acting like a focusing quadrupole magnet) and then drifts during the bunch spacing time. The bunch-train gap can be represented by a long drift period. Therefore, we can obtain the one turn transportation matrix of the ion motion. When a gap τ_{gap} is applied with a bunch train length τ_{train}, the stable condition of the ion's linear motion becomes [28]

$$n\pi < \theta < n\pi + 2arctg\frac{2}{\omega_i \tau_{gap}}, \tag{27}$$

where $\theta = \omega_i \tau_{train}$. With the increment of the gap, the unstable region increases as shown in Fig. 10. A gap of one period of ion oscillation already provides a large unstable zone (more than 60%). The unstable zone increases dramatically with a gap of 1~2 ion oscillation period and then slows down with further increment of the bunch-train gap. This is consistent with the exponential decay of the ion-cloud given by simulation and experiment.

The minimum required train gap is a few of ion's oscillation periods. There is a small ion's oscillation period for a high beam current with a small emittance. Therefore, a shorter train gap is needed to clear the

ions for higher intensity beams. In other words, the bunch train gap is more effective for high intensity beams with small emittance.

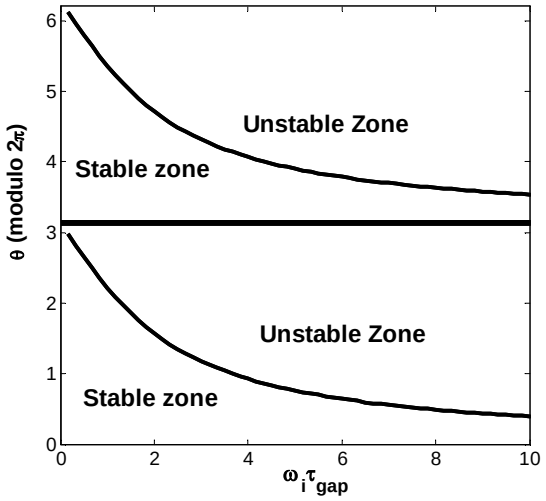

FIG. 10. Variation of stable and unstable zones with the length of the bunch train gap

Reduction of ion density by using multi-bunch train beam filling

The exponential decay makes it possible to effectively reduce the trapped ions by using a multi-bunch train beam filling pattern with a short train gap. This works especially well for high intensity beams. We assume there are N_{train} bunch-trains evenly distributed along the ring. Each bunch-train consists of M bunches and followed by a bunch train gap τ_{gap}. The density of ion-cloud during the bunch-train gap exponentially decays with a decay time of $\tau_{diffusion}$, which is order of the ion oscillation period. Therefore, the ion density after the passage of n_{th} bunch-train becomes

$$\rho_n = gMN_e \sum_{k=0}^{n-1} \exp(-k\tau_{gap}/\tau_{diffusion}), \tag{28}$$

Here g is a constant parameter for given vacuum pressure and beam size

$$g = \delta_i \frac{P}{kT} \frac{1}{k_y \sigma_y (\sigma_x + \sigma_y)}. \tag{29}$$

After a long enough period of time, the ion density reaches saturation level at

$$\rho_\infty = gMN_e \frac{1}{1 - e^{-\tau_{gap}/\tau_{diffusion}}}. \tag{30}$$

With this scheme, the density of trapped ions can be significantly reduced compared to a long single train filling pattern by a factor

$$f_{gap} = \frac{\rho_\infty}{gMN_{train}N_e} = \frac{1}{N_{train}} \frac{1}{1 - e^{-\tau_{gap}/\tau_{diffusion}}}, \qquad (N_{train} << n_b). \tag{31}$$

It can be concluded from the above equation that the multi-bunch-trains filling is an effective way to reduce the ion density in a large storage ring (therefore a large N_{train}) with a low emittance (short $\tau_{diffusion}$). In electron rings, the vertical emittance is smaller than the horizontal emittance and therefore the vertical motion of the ions with gaps become unstable first. Strictly speaking, Eq. (31) is valid for beams with large aspect ratios where the short gaps destabilize only the vertical ion trapping. One can multiply the left side of Eq.(31) by a similar factor due to the horizontal decay of the ions if the gap length is not negligible compared to the ion's horizontal oscillation period.

The number of bunches in the electron damping ring of the International Linear Collider (ILC) varies from 3000 to 6000 [29]. Fig. 11 shows the build-up with 5782 total number bunches. There are 118 bunch trains and each bunch train consists of 49 bunches followed by train gap of 38 *ns*. The ion density near the beam saturates after about 7 bunch trains and it is reduced by a factor of 60 compared to the single bunch train filling pattern. The beam-ion instability mainly depends on the ion-cloud near the beam. Therefore, there is a significant reduction of the instability growth rate by applying the multi-bunch train filling pattern.

For a given circumference of the accelerator ring, the f_{gap} can be minimized by choosing different N_{train} and $\tau_{gap.}$ The saturated ion density after long enough of period of time can be found for each beam filling pattern by simulation as Fig. 11 shown. By this way, we can get the saturated ion density dependence on the beam filling pattern by simulation. Fig. 12 shows the variation of ion density near the beam in the ILC damping ring with the number of bunch trains by simulation and the calculated f_{gap} from Eq. (31). The density is normalized by the density of one long bunch train filling pattern case. Therefore, the density has the same meaning as f_{gap}. The simulation agrees very well with the analysis. It shows that the ion-density can be effectively reduced with about 50 bunch-trains. The reduction speed becomes slow with a further increment of the bunch-train number due to a shorter train gap.

A multi-bunch-train filling pattern is a combination of uniform beam filling (with a constant ion density) and single bunch-train filling pattern where the ion density linearly increases along the bunch train. The instability growth rate is proportional to the average ion density seen by the beam. We define the ratio of the average ion density to the maximum ion density as

$$a = \bar{\rho} / \rho_{\infty}, \qquad (0.5 \le a \le 1) \ . \tag{32}$$

Then the growth rate with a multi-bunch-train filling pattern can be written as

$$\frac{1}{\tau} \approx \frac{a r_e c \beta_y \rho_{\infty} Q}{\gamma}, \quad (0.5 \le \quad \le 1). \tag{33}$$

The above equation can be considered to be the instability growth rate for a general beam filling pattern with a=1 for an even beam filling pattern and a=1/2 for a single bunch train beam filling pattern.

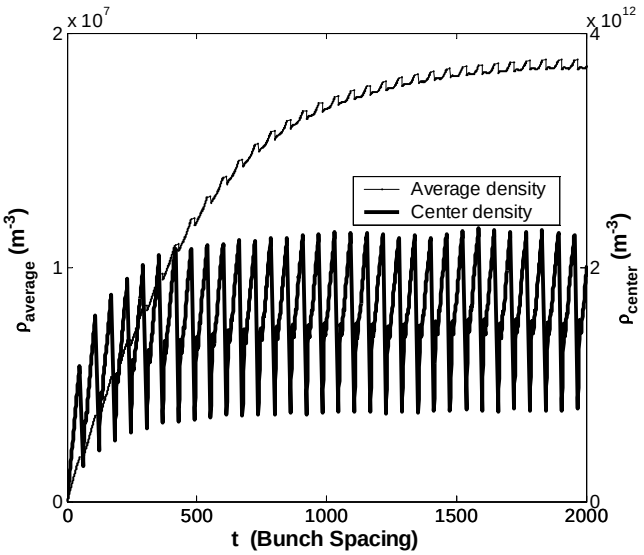

FIG. 11. Build-up of CO+ ion-cloud in ILC damping ring. The pressure is 1nTorr, horizontal emittance is 0.5 *nm* and vertical emittance is 2 *pm*. The bunch spacing is 3 ns. The average density is the density over the whole beam pipe, and the density near the beam is the ion density within $\sqrt{3}$.

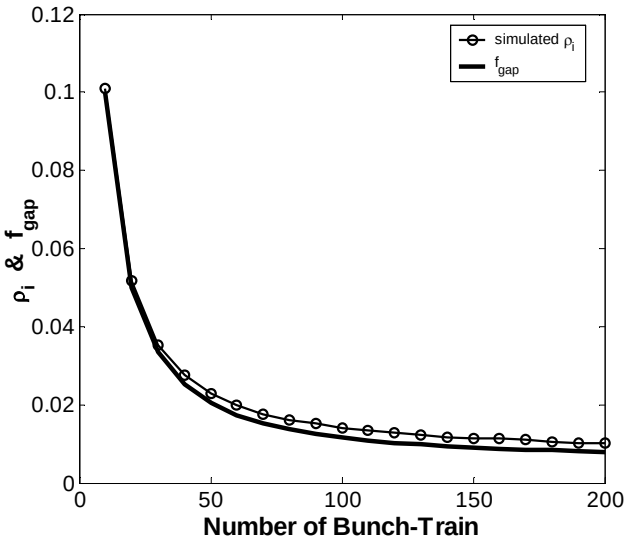

FIG. 12. Normalized ion-density near the beam for various numbers of bunch-trains by simulation and analysis. The density is normalized by the density of one long bunch-train filling pattern. The total number of bunches, bunch current and bunch spacing are the same while the bunch train gap is adjusted to keep the length of the ring constant. A diffusion time of 22.7 *ns*, which is equal to the ion oscillation period, is used in the calculation of f_{gap}.

Simulation of beam instability with multi-bunch train filling

Simulation has a number of advantages in the study of the beam-ion instability: the nonlinearity of the ion-cloud is automatically included; the effects of optics and bunch-train gap with arbitrary beam filling pattern can be easily handled; a realistic vacuum model with multi-gas species is straightforward in simulation, etc.

There are two simulation codes in SLAC. One is based on so called strong-strong model. Both the ions and high energy bunches are represented by many macroparticles. Therefore it can simulate both the dipole instability and beam emittance blow-up. Another code is based on weak-strong model. The ion-cloud is represented by many marcoparticles, but the high energy bunch is represented by one macroparticle with rigid transverse bunch profile. As a result, this type of code can't be used to simulate the emittance growth. A weak-strong code is used in this paper in order to speed-up the simulation.

The ions are distributed along the whole ring. The optics of the ring with MAD [30] type of format is read as an input of the code. New ions are generated in each element when electron bunches pass by. The ions generated by previous bunches will receive a kicker from the following bunches. Meanwhile the electron bunch also receives a kicker from the ion-cloud in each element. The space-charge field of ion cloud is calculated based on the particle in cell (PIC) method. The field of high energy bunches is calculated using Bassetti-Erskine formal [31] (as shown in appendix A) in the weak strong model and numerical method in the strong and strong model. The electron bunches are tracked through the accelerator element-by-element, and therefore, the modulation of the ion oscillation frequency due to the variation of the beam size is automatically taken into account.

Multi-gas species, including H_2, CH_4, H_2O, CO and CO_2, are used in the code to represent the realistic vacuum pressure. Different types of ions are generated in each element according to the partial pressure and ionization cross-section of the gas species.

Several examples are given in this section. The first one is the ILC electron damping ring. It is a 6 *km* ring with beam energy of 5 GeV. The main parameters are listed in Table 1. Fig. 13 shows the simulated beam's vertical instability in the ILC damping ring for different bunch-train numbers with a total of 5782 bunches. A partial vacuum pressure of 1nTorr (CO^+) is used. It clearly shows the mitigation of the beam instability by using multi-bunch train beam filling as predicted in Fig. 12.

Fig. 14 shows the beam instability with the same filling pattern as Fig. 11. The beam has 118 bunch trains. There is no clear improvement of the instability with further increase of the number of bunch-trains because the train gap becomes shorter with an increasing number of bunch-trains. This agrees with the slow change of ion density with the number of bunch trains when N_{train}>180 as shown in Fig. 12. The beam amplitude grows exponentially when the amplitude is small compared to the beam size, and then the growth is slowed down by the nonlinearity at large amplitude. The exponential growth time is about 0.26 *ms*. Simulation with the averaged constant beam size shows a growth rate of 3.25 times faster than the growth rate with real optics. This indicates that the real optics provides a Landau damping due to the ion frequency spread. Many unstable modes are excited due to the variation of ion's frequency along the ring

even with single gas species CO^+ as shown in Fig. 14. Note that there can be multiple unstable modes even with a constant beam size because of the low *Q* and high frequency of the wake

$$\mathrm{n}_{\mathrm{mod}\,e} = \frac{\Delta\omega}{\omega_0} \approx \frac{\omega_i}{Q\omega_0} >> 1. \tag{34}$$

For ILC damping ring, the beam emittance varies with time. The equilibrium emittance is used in the above study. With a larger emittance, ions are easier to be trapped (trapping condition) and the train gaps are less effective in the clearing of ions (long decaying time). As a result, more ions can be accumulated and a higher ion density can be achieved for a fixed beam filling pattern [19]. The trapped ion density is not a monotonic function of emittance in ILC case. There are two advantages for ultra small emittance like ILC: fast decay of the ions during the gaps and unstable motion of light ions. For instance, Hydrogen ion becomes unstable with the ultra small emittance of ILC. In this paper the ion motion within the bunch train is assumed to be stable

$$A > \frac{N_e r_p S_b}{2(\sigma_x + \sigma_y)\sigma_y}. \tag{35}$$

With a fixed multi-bunch train filling, the instability with a lower emittance is not always stronger due to the complexity of the ion motion although it is stronger in most cases. For instance, there is no beam ion instability in extreme case with a high intensity beam and an extreme low emittance because ions are unstable even within single bunch train (see Eq.35). Therefore, the stability of the ion motion should be checked first. In short summary, the optimized filling pattern depends on the gas species, emittance, optics and beam current.

The second example is SuperKEKB, which is the upgrade plan of KEKB factory. Two options are listed in Table I. In this paper we estimate the instability of the high charge option only. Unlike KEKB, the electron beam may be stored in LER at SuperKEKB in order to mitigate the electron cloud effect. In this case, the beam energy is decreased from 8 to 3.5 *GeV* and the beam current is increased from 1.1 to 9.4 *A*. The vacuum pressure in beam chambers will be increased from 1 to 5 *nTorr* due to the large stored current. All factors contribute to an enhancement of the ion effects. The ion instability for high charge mode is about 19 times stronger than present KEKB. It will be 24 times stronger in the low charge mode. Low charge mode is chosen in the current design. The ion effects can be strong enough to degrade the luminosity.

Systematic scan of the beam filling pattern has been done in order to optimize the filling pattern. Fig. 15 shows the growth rate for various beam filling patterns with a partial pressure of CO^+ 1 *nTorr*. It clearly shows the mitigation of instability with a longer train gap and shorter train. The simulated growth rate for a fixed bunch-train gap is proportional to the number of bunches per train. There is a similar total bunch number n_b for these filling patterns. As a result, the ion density near the beam, and therefore the instability growth rate, is approximately proportional to the number of bunches per bunch-train *M*

$$\mathrm{f}_{gap} = \frac{1}{n_b}\frac{M}{1-\exp(-\tau_{gap}/\tau_{diffusion})} \propto M. \tag{36}$$

The simulation agrees well with the above relation.

It is more interesting that the simulated growth rate for different beam filling patterns in SuperKEKB follows the scaling law

$$\frac{1}{\tau_{Super\_KEKB}} = 0.59\frac{r_e c\bar{\beta}_y \rho_{ic}}{\gamma} \quad . \tag{37}$$

Here ρ_{ic} is the maximum ion density near the beam $\rho_{ic} \approx k_y \rho_\infty$. An average betatron function is used. The factor Q, which includes both the nonlinear force and optics effects, is included in the coefficient 0.59. Comparing this scaling law with Eq. (33), it can be concluded that the factor Q in SuperKEKB is smaller than 2, which indicates that the frequency spread due to variation of the beam size along the ring provides an effective damping of the instability.

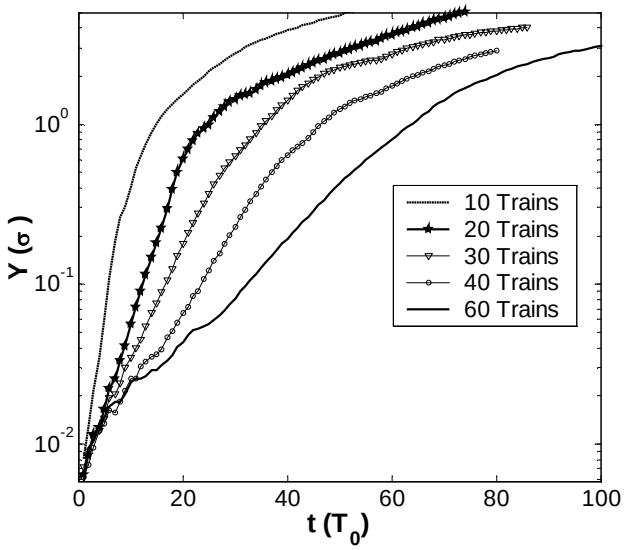

FIG. 13. Growth of the beam's vertical amplitude for various ILC beam filling patterns. The revolution period T_0 is 20μs. The amplitude is normalized by vertical beam size. The total number of bunches is 5782 and the vacuum pressure is 1 *nTorr* of CO^+.

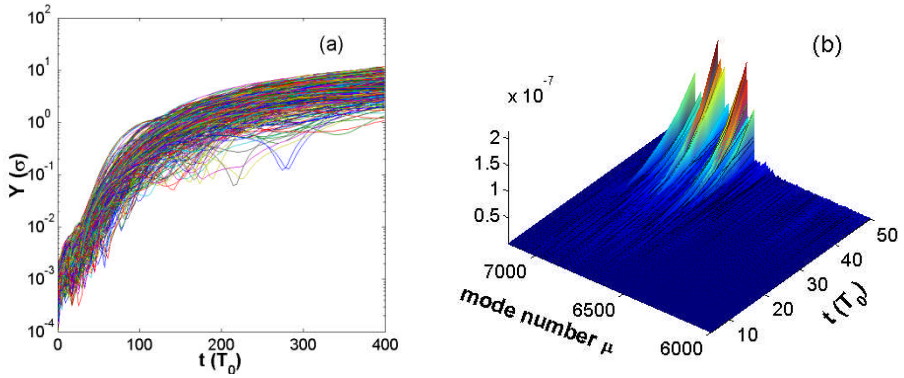

FIG. 14. Simulated vertical oscillation amplitude of different bunches (a) and the unstable modes (b) in ILC electron damping ring. The amplitude is normalized by the beam size. There are 118 bunch trains.

Each bunch train consists of 49 bunches followed by a bunch-train gap of 43 *ns*. The bunch spacing is 3 *ns* and bunch intensity is 1×10^{10}. The pressure is 1 *nTorr* of CO^{+}.

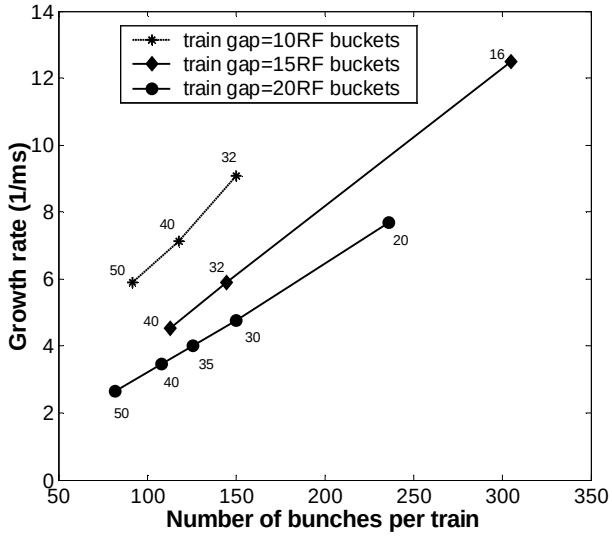

FIG. 15. Instability growth rate in SuperKEKB (high charge option) as a function of the number of bunches per bunch train for different train gaps of 10, 15 and 20 buckets. The pressure is 1 *nTorr* of CO+. The number of bunch-trains is also shown in the plot.

Observation of Beam-ion instability in SPEAR3 with multi-bunch train beam filling pattern

SPEAR3 has a circumference of 234 m with a harmonic number of 372. The normal beam filling pattern is a single bunch train with 280 bunches followed by a gap of 92 RF buckets spacing. The natural emittance is 10 nm and there is a low vertical emittance of 14 *pm*. With a larger vertical emittance (by changing coupling), the observed frequency of the sidebands becomes lower and the peak amplitude of the sidebands also decreases (not shown here). The couple bunch instability driven by impedance, for instance the resistive wall impedance, does not change with the beam size. Furthermore, the impedance of resistive wall decreases as $1/\sqrt{\omega}$, which is not observed. Therefore, the change of the sideband with emittance directly confirms that the observed instability is caused by the ions in the vacuum. The observed frequency of the sideband agrees with the analysis and increases with beam current as expected. Moreover, we experienced strong vertical beam instability and beam loss when there was a vacuum burst due to the flash at titanium sublimation pumps (TSPs). And the beam loss time correlates with pressures rise. Many evidences convince us the instability in SPEAR3 is driven by ions. We have observed the vertical lower

sideband from the beam spectrometer for different beam filling patterns with a total beam current of 500 *mA*. Fig. 16 shows the vertical oscillation amplitude at each sideband estimated from the beam spectrometer signal for one, four and six bunch-train beam filling patterns. It clearly shows that the multi-bunch train filling pattern can significantly mitigate the instability. The instability becomes very weak with the six bunch-trains filling pattern. The dominant gas species in SPEAR3 are Hydrogen, Methane, Water, Carbon monoxide, Carbon Dioxide. Among them, Hydrogen ion has the largest frequency about 70MHz due to its small mass number and Carbon Dioxide has low frequency below 10MHz.

Beam-ion instability is also observed with normal operation current of 200 *mA* [32]. In 200 *mA* operation mode, the sideband completely disappears with a two bunch-trains filling pattern. A complete description of the comprehensive observation of the beam ion instability in SPEAR3 will be presented in a separated paper soon.

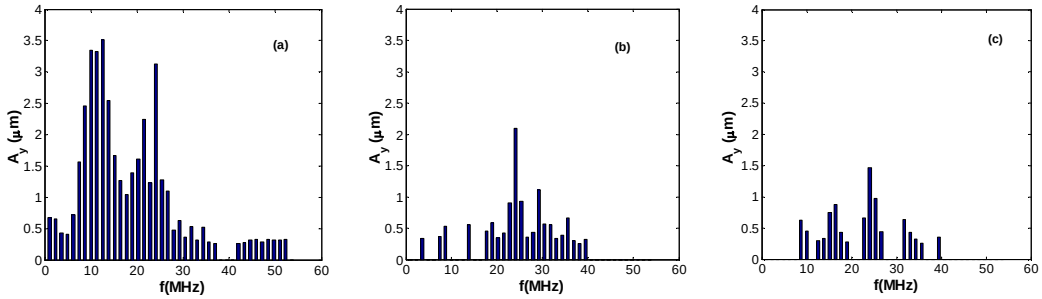

FIG. 16. Measured beam's vertical lower sideband for different beam filling patterns: (a) one bunch train; (b) four bunch train; (c) six bunch train. The total beam current is 500 *mA* with total bunch number of 280 in all cases.

V. COHERENT TUNE SHIFT AND BUNCH-BY-BUNCH FEEDBACK

In this section, we briefly discuss another two important aspects: coherent tune shift due to ions and the suppression of ion instability using an active feedback system.

The focusing force of trapped ions causes a positive tune-shift to the electron bunches

$$\Delta \nu_y = \frac{\beta_y}{4\pi}\frac{\partial \Delta y_e'}{\partial y_e} = \frac{r_e}{3\pi\gamma}\int_{ion\ trapped\ \text{region}} \frac{\beta_y \lambda_{ion}}{\sigma_y(\sigma_x+\sigma_y)} ds\,. \tag{38}$$

If the tune shift is too large, it may degrade the performance of the accelerator [33]. Similar to the instability growth rate, the tune shift is also proportional to the ion density. Therefore, the tune shift of

electron bunches for a single bunch-train filling pattern linearly increases along the bunch train. The ion-cloud is assumed to be stable in the derivation of the above equation. The simulated tune shift is a perfect linear function of bunch number when the beam is stable and agrees well with analysis as shown in Fig. 17. Each time only one test electron bunch oscillates under the ion-cloud force. Other bunches are stabilized by a bunch-by-bunch feedback system. By this way we can get the tune of the test bunch in each simulation.

When the beam is unstable, the tune shift depends on the coupled motion between the electron beam and ion-cloud. Fig. 18 shows the dependence of the tune-shift on the coupled motion in the linear regime where the amplitude of beam oscillation is smaller than the beam size. For instance, when all electron bunches have the same phase (0-mode), the ion-cloud doesn't oscillate coherently and causes the smallest tune shift. On the other hand, when the k_{th} electron bunches has initial phase $\phi_k(t=0) = \phi_0 + \omega_i k S_b / c$ (resonance mode), the ion-cloud oscillates resonantly with the electron beam and causes the largest tune-shift to the electron beam. It can be a few times larger than that given by Eq. (38).

However, the tune-shift is quite different in the nonlinear regime when the amplitude of electron beam is larger than its transverse beam size because the instability significantly changes both the distribution and density of the ion-cloud. Simulation shows that the tune shift of the resonance mode becomes comparable with Eq. (38) in the nonlinear region. Note that only the tune-shift in nonlinear regime can be observed without feedback. The tune shift with an unstable beam is complicated and will be addressed separately elsewhere.

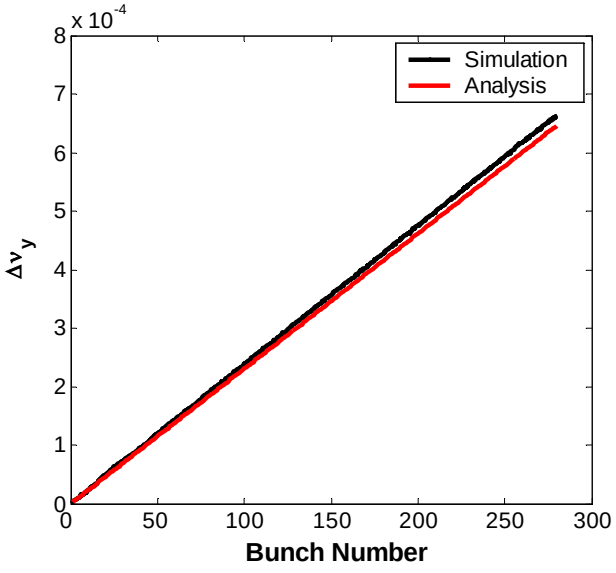

FIG. 17. Simulated vertical tune shift along the bunch train for SPEAR3 beam with a partial pressure of 1*nTorr* CO^+. The beam has a single bunch train with total number of 280 bunches. A fast bunch-by-bunch feedback can be applied to stabilize the beam. When feedback is turned off, the tune shift varies with time.

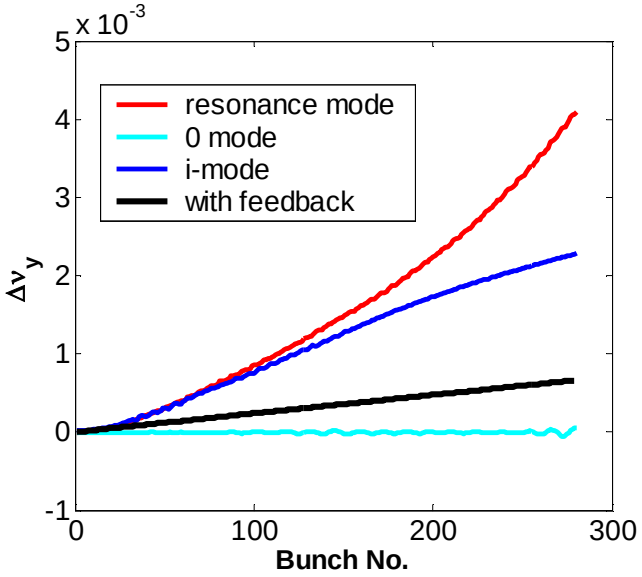

FIG. 18. Dependence of vertical tune shift along the bunch train on the coupled motion in the linear regime. Here i-mode is one of the modes other than 0 and resonance modes.

A better vacuum can directly reduce the growth rate of the instability, however, the improvement is limited and the cost can be prohibitive. A bunch-by-bunch feedback can be used to completely suppress the instability. Simulation shows that a feedback with a damping time shorter than the exponential growth time is required. Fig. 19 shows the damping of the beam instability by a bunch-by-bunch feedback system. The feedback is initially turned off and turned on at 52th turn. The growth is finally damped by the feedback system. There are five gas species in the vacuum. Therefore, several groups of unstable modes are shown up in the figure. A semi-analytical study also confirms that a feedback with a damping time of the same level as exponential growth time seems enough to damp the instability to the noise level [33]. When a feedback system with damping time of a few tens of turns is required, there may be issues associated with noise within the feedback system itself. Specifically, noise in the pickup or amplifier may be transferred to the kicker, which then induces some jitter on the beam. The net result of the feedback is that the beam will

reach certain *rms* oscillation amplitude which is determined by the feedback damping and noise [34]. The experiment in SPEAR3 [32] shows that a bunch-by-bunch feedback system can effectively damp the beam ion instability.

The growth rate of single bunch train instability (FII) increases along the bunch train. Therefore it is expected that a slow feedback can damp bunches in the head of the bunch train first and then gradually stabilizes the whole bunch train. This is only true for ideal case without any jitter and errors. In reality, a slow feedback with a damping time longer than the exponential growth time can only damp the non-linear instability and reduces the beam's oscillation amplitude to the order of beam size. Therefore, the beam seems stable even with a slow feedback. However, the remaining oscillation can still quietly degrade the beam quality.

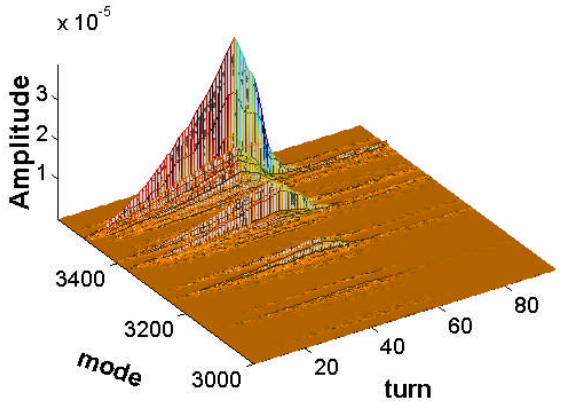

FIG. 19. Simulated damping of beam instability in ILC damping ring using a bunch-by-bunch feedback. The total number of bunches is 2767. There are 125 bunch trains. Each bunch train consists of 22 bunches followed by a bunch-train gap of 38 *ns*. The bunch spacing is 6 *ns* and bunch intensity is 2.0×10^{10}. There are five gas species including Hydrogen, Methane, Water, Carbon Monoxide and Carbon Dioxide. Each type of gases has the same partial pressure and the total pressure is 1 *nTorr*. The feedback is initially turned off and turned on at the 52^{th} turn.

VI. CONCLUSIONS

The suppression of beam-ion instability using a multi-bunch train filling pattern is systematically studied. It is an effective mitigation for high intensity beams with a low emittance. Simple formulae are

derived for the build-up of ion clouds (Eq.30) and growth rate of the instabilities with a general beam filling pattern (Eq.33).

Both the distribution and electric field of trapped ions are benchmarked with numerical approach. The distribution of ion cloud has a sharp peak near the center and its dimension is smaller than the electron bunch from which the ions are born. The electric field of the ion-cloud closely approximates that of a Gaussian distribution with $\sigma_i^2 \approx \sigma_e^2 / 2$.

A wake field model is introduced to study the beam ion instability in the exponential growth region. The simulated wake agrees reasonably with the analysis model. The total wake field of an ion-cloud along the whole ring is proportional to the ion density and the circumference of the ring. The wake field of ion cloud with a flat beam is inversely proportional to the 1.5 power of the product of horizontal and vertical beam size. Therefore, the beam-ion instability can be very strong for future ultra-small emittance rings.

We briefly discuss the beam ion instability growth rate with different beam filling patterns: uniform beam filling, single bunch-train filling and multi-bunch-train filling. It is interesting that the maximum exponential growth rate in all cases is proportional to the average ion density near the beam seen by the electron bunches.

Both simulation and experiment found that the ion cloud exhibits exponential decay during the bunch-train gap with an exponential time constant of the order of the ion's oscillation period. This phenomenon can be explained by the characteristics of the motion of the ion particle. This feature makes the multi-bunch train filling pattern a very effective way to reduce the ion density for an electron ring with high beam current and low emittance. The reduction of the ion density can be up to two orders of magnitude. Several examples are given and there is good agreement between the analysis and simulation. The observation from SPEAR3 also directly confirms the effectiveness of the multi-bunch-train filling pattern on suppression of the beam instability.

The trapped ions induce a positive coherent tune shift. With an unstable beam, the tune shift is sensitive to the coupled mode of electron beam and it dynamically changes with time. When the beam is stabilized by a feedback system, the ion-induced tune shift agrees well with the analysis.

A bunch-by-bunch feedback with a damping time shorter than the exponential growth time is required to completely damp the instability. A slow feedback can only damp the non-linear instability and reduce the beam oscillation amplitude to the order of the beam size.

ACKNOWLEDGMENTS

We would like to acknowledge the SPEAR3 team for its help on the SPEAR3 observations, with special thanks to J. Safranek for his support and contributions. The author Wang would like to thank A. Chao, K. Ohmi and M. Takao for fruitful discussions, G. Stupakov for reading the manuscript, M. Boland at AS and A. Streun at SLS for providing the parameters of the rings.

APPENDIX A: TRANSVERSE DISTRIBUTION OF IONS

The ion's distribution without beam instability is discussed here. The ions are born from the electron bunches in our case. Therefore they have the same distribution as the electron bunch when they are born. Then the ions move under the potential of electron bunches. For most of electron rings, the self space charge of ions is negligible comparing with the electron-beam's space charge. The electric field of a bi-Gaussian beam is

$$E_x = \frac{eN_e}{2\pi\varepsilon_0} x \int_0^\infty \frac{\exp[-\frac{x^2}{2\sigma_x^2+t} - \frac{y^2}{2\sigma_y^2+t}]}{(2\sigma_x^2+t)^{3/2}(2\sigma_y^2+t)^{1/2}} dt = \frac{eN_e}{4\pi\varepsilon_0}\sqrt{\frac{2\pi}{\sigma_{e,x}^2-\sigma_{e,y}^2}}\,\mathrm{Re}\big[f(x,y)\big], \qquad \text{(A.1)}$$

$$E_y = \frac{eN_e}{2\pi\varepsilon_0} y \int_0^\infty \frac{\exp[-\frac{x^2}{2\sigma_x^2+t} - \frac{y^2}{2\sigma_y^2+t}]}{(2\sigma_x^2+t)^{1/2}(2\sigma_y^2+t)^{3/2}} dt = \frac{eN_e}{4\pi\varepsilon_0}\sqrt{\frac{2\pi}{\sigma_{e,x}^2-\sigma_{e,y}^2}}\,\mathrm{Im}\big[f(x,y)\big], \qquad \text{(A.2)}$$

$$f(x,y) = w\left(\frac{x+iy}{\sqrt{2(\sigma_{e,x}^2-\sigma_{e,y}^2)}}\right) - \exp\left(-\frac{x^2}{2\sigma_{e,x}^2} - \frac{y^2}{2\sigma_{e,y}^2}\right) w\left(\frac{x\frac{\sigma_{e,y}}{\sigma_{e,x}} + iy\frac{\sigma_{e,x}}{\sigma_{e,y}}}{\sqrt{2(\sigma_{e,x}^2-\sigma_{e,y}^2)}}\right), \qquad \text{(A.3)}$$

$$w(z) = e^{-z^2}\left[1 + \frac{2i}{\sqrt{\pi}}\int_0^z e^{t^2} dt\right], \quad z = x+iy. \qquad \text{(A.4)}$$

Where $\sigma_{e,x,y}$ is the transverse root mean square (*rms*) beam size and N_e is the bunch population. When $x < \sigma_{e,x}$ and $y < \sigma_{e,y}$, there is a linear field

$$\begin{bmatrix} E_y \\ E_y \end{bmatrix} = \frac{eN_e}{2\pi\varepsilon_0\sigma_{e,x,y}(\sigma_{e,x}+\sigma_{e,y})}\begin{bmatrix} x \\ y \end{bmatrix}. \qquad \text{(A.5)}$$

The motion of ions in horizontal and vertical directions is decoupled in the linear regime. Here we consider the horizontal motion only. With the field given by Eq. (A.5), the motion equation of an ion can be written in the form

$$\ddot{x} + \omega_{x0}^2 x = 0 . \tag{A.6}$$

A good approximation is obtained by assuming that the ions are born at rest since the beam's potential (up to *keV* level) is much larger than the ions' thermal energy (less than 1*eV*). Therefore the solution of horizontal motion is

$$x(t) \approx x_0 \sin(\omega_{x0} t + \phi_0) . \tag{A.7}$$

Where x_0 is the ion's oscillation amplitude, which is approximately the position at its birth. ϕ_0 is the ion's initial phase when the ions are born, which has a uniform distribution due to the random generation of ions (time). Therefore, the ions born at x_0 has the following distribution in x

$$f(x, x_0) = \frac{2}{\pi\sqrt{x_0^2 - x^2}}, \quad (x<x_0). \tag{A.8}$$

The initial position of ions x_0 has a Gaussian distribution with the same dimension as the electron bunch

$$\rho_0(x_0) = \frac{1}{\sqrt{2\pi}\sigma_{e,x}} \exp\left(-\frac{x_0^2}{2\sigma_{e,x}^2} \right). \tag{A.9}$$

Therefore the distribution of ions at the equilibrium becomes

$$\rho(x) = \int_x^\infty f(x, x_0)\rho_0(x_0)dx_0 = \frac{1}{\pi\sqrt{2\pi}\sigma_{e,x}} e^{-\frac{x^2}{4\sigma_{e,x}^2}} K_0\left(\frac{x^2}{4\sigma_{e,x}^2} \right), \tag{A.10}$$

where K_0 is the modified Bessel Function of the Second Kind and its asymptotic forms is

$$K_0(x) \approx \begin{cases} -\ln\frac{x}{2} - \gamma_c & x \to 0 \\ \sqrt{\frac{\pi}{2x}} e^{-x} & x \to \infty \end{cases} . \tag{A.11}$$

Where the constant $\gamma_c = -\int_0^\infty e^{-x} \ln x dx = 0.5772156649$. With the asymptotic form, the ion-distribution near the beam center is

$$\rho(x) \approx -\frac{1}{\pi\sqrt{2\pi}\sigma_{e,x}} e^{-\frac{x^2}{4\sigma_{e,x}^2}} \left(\log(\frac{x^2}{8\sigma_{e,x}^2}) + \gamma_c \right) . \tag{A.12}$$

Eq.(A.10) and (A.12) gives the one-dimension ion distribution at the equilibrium. The same result of Eq. (A.10) was first given by Tavares [15]. But the asymptotic form in [15] is incorrect.

Because self space charge of ions and their thermal energy are negligible, the distribution of ion-cloud is only decided by the electron bunch from which the ions are born. Fig. A1 shows the horizontal distributions of an electron bunch and the ions born from the electron bunch. The ion distribution has a sharp peak near the center and its dimension is smaller than the electron bunch. Surprisingly, the asymptotic form agrees very well within two *rms* beam size, where most of ions are trapped. Therefore, the asymptotic form is good enough to express the ion distribution.

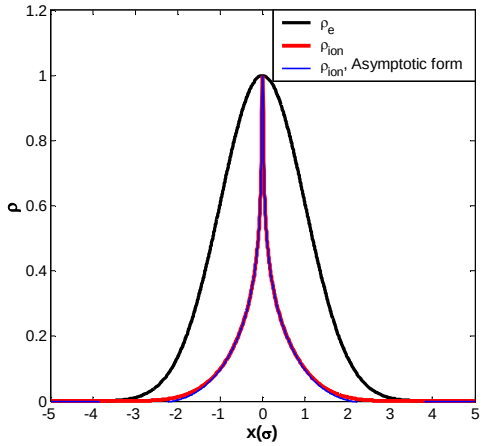

FIG. A1. One dimensional distribution of an ion-cloud and the electron bunch. The ion distribution with asymptotic forms also is shown. The horizontal axis is in unit of the *rms* beam size.

REFERENCES

[1] J. Byrd, et al., Phys. Rev. Lett. 79, 79(1997)

[2] J. Y. Huang, et al., Phys. Rev. Lett. 81, 4388 (1998)

[3] M. Kwon et al., Phys. Rev. E 57, 6016 (1998)

[4] K.Y. Ng and M. Popovic, FERMILAB-FN-0712 (2001)

[5] S.J. Werkema, K.D Fullett and P. Zhou, in *Proceedings of the 1993 Particle Accelerator Conference, Washington DC*, p3309 (1993)

[6] T.O. Raubenheimer and F. Zimmermann, Phys. Rev. E52, No. 5, 5487 (1995)

[7] G.V. Stupakov, T.O. Raubenheimer, F. Zimmermann, Phys. Rev. E52, 5499 (1995)

[8] G. V. Stupakov, KEK Proceedings 96-6, 243 (1996)

[9] K. Ohmi, Phys. Rev. E55, 7550 (1997)

[10] E. Bozoki and D. Sagan, Nucl. Instrum. Meth. A340, 259(1994)

[11] M. Zobov, Journal of Instrumentation 2, P08002 (2007)

[12] L. Wang, T.O. Raubenheimer and A. Wolski, in *Proceeding of 2006 European Particle Accelerator Conference, Edinburgh, UK*, p2155 (2006)

[13] G. Xia and E. Elsen, Nucl. Inst. Methods, A593, 183 (2008)

[14] E.S. Kim and K.Ohmi, Japanese Journal of Applied Physics 48, 086501 (2009)

[15] P.F. Tavares, CERN PS/92-55 (LP) (1992) (unpublished)

[16] K. Ohmi and F. Zimmermann, Phys. Rev. E65, 016502 (2001)

[17] K. Ohmi and F. Zimmermann, Phys. Rev. Lett. 85, 3821 (2000)

[18] Alexander W. Chao, *Physics of Collective Beam Instabilities in High Energy Accelerators* (Wiley, New York, 1993).

[19] L. Wang, Y. Cai, and T. O. Raubenheimer, in *Proceedings of 2007 Particle Accelerator Conference, Albuquerque, USA*, 4240(2007)

[20] H. S. Kang, et. al., in *Proceeding of 2006 European Particle Accelerator Conference, Edinburgh, UK*, 2771(2006)

[21] R. Nagaoka, et al., in *Proceedings of 2007 Particle Accelerator Conference, Albuquerque, USA*, 2019(2007)

[22] B. Jiang, et. al., Nucl. Instrum. Meth. A 614, 331(2010)

[23] D. J. Peake, et.al., in *Proceedings of 2009 Particle Accelerator Conference, Vancouver, Canada*, 4105(2009)

[24] R. Hettel, et. al., in *Proceedings of 2009 Particle Accelerator Conference, Vancouver, Canada*, 2297(2009)

[25] R.A. Bosch, Nucl. Instrum. Meth. A450 223(2000).

[26] S. Heifets, et. al., SLAC-PUB-12959, 2007

[27] M. Takao, et. al, in *Proceedings of 2002 European Particle Accelerator Conference, Paris, France*, 1562(2002)

[28] D. Sagan and A. Temnykh, Nucl. Instrum. Meth. A344, 459 (1994)

[29] N. Phinney, N. Toge and N. Walker, International Linear Collider Reference Design Report, Vol. 3, 2007, http://www.linearcollider.org/about/Publications/Reference-Design-Report

[30] H. Grote and F. Schmidt, in *Proceedings of 2003 Particle Accelerator Conference, Portland, USA*. 3497(2003)

[31] M. Bassetti, G.A. Erskine, CERN-ISR-TH/80-06.

[32] L. Wang, et. al., to be presented in The 2011 International Particle Accelerator Conference, San Sebastian, Spain(2011)

[33] H. Fukuma and L. Wang, in Proceedings of ECLOUD'07, April 9-12, 2007, Daegu, Korea. And also SLAC-PUB-12757.

[34] A. W. Chao and G. V. Stupakov, KEK Proceedings 97-17, 110 (1997).